SciMedCentral

JSM Nanotechnology & Nanomedicine

Research Article

A Study of Localized Surface Plasmon Resonance Nanoslit Array and Applications for Chip-based Protein Detection

Jianjun Wei[1]*, Matthew Kofke[2], Sameer Singhal[3] and David H. Waldeck[2]*

[1]*Department of Nanoscience, Nanoengineering, University of North Carolina, USA*

[2]*Department of Chemistry, University of Pittsburgh, USA*

[3]*Department of Biomedical & Energy Division, CFD Research Corporation, USA*

Abstract

Ordered arrays of nanostructures in thin metal (Au) films have been studied for localized surface plasmon resonance (LSPR) sensing with a transmission spectral mode. We report on a nanoslit array device that is designed to permit extraordinary optical transmission (EOT) with a tunable primary peak in the visible to near infrared range and a spectral shape and light transmission that is determined by surface plasmon manipulation in the embedded gold film. Finite-difference time-domain (FDTD) simulation studies show that a nanoslit array device can provide a well-defined transmission resonance and display a monotonically increasing value of the resonance peak wavelength, λ_{max}, with increasing period. Simulation studies show that the refractive index (RI) changes occurring on the in-slit gold surfaces contribute the most to the resonance transmission wavelength shift, suggesting that the strong confinement of LSPR in the narrow slit region is the origin of the sensitive RI response. These planar nanoslit array devices were used to detect the ligand binding protein, β-lactoglobulin (β-LG), with functionalization of specific binding retinals linked via a self-assembled monolayer at the array surfaces. These results illustrate the promise of nanoslit arrays for LSPR bio-detection in a lab-on-chip device platform.

Special Issue on

Research at the Joint School of Nanoscience and Nanoengineering

Corresponding authors

Jianjun Wei, Department of Nanoscience, University of North Carolina, USA, Tel: +1-336-285-2859; Fax: +1-336-500-0115; E-mail: j_wei@uncg.edu

David H. Waldeck, Department of Chemistry, University of Pittsburgh, USA, Tel: +1-412-624-8430; Fax: +1-412-624-8611; Email: dave@pitt.edu

Submitted: 22 August 2014

Accepted: 27 August 2014

Published: 29 August 2014

Keywords

- Localized surface plasmon resonance (LSPR)
- Nanoslit array
- Optical transmission
- Biosensor

ABBREVIATIONS

EBL: Electron-Beam Lithography; **EOT**: Extraordinary Optical Transmission; **FDTD**: Finite-Difference Time-Domain; **FIB**: Focus Ion Beam; **LSPR:** Localized Surface Plasmon Resonance; **LOC**: Lab-On-Chip; **PBS**: Phosphate Buffer Saline; **RI**: Refractive Index; **RIU**: Refractive Index Unit; **LG**: Lactoglobulin, **SAM**: Self-Assembled Monolayer

INTRODUCTION

Lab-on-chip (LOC) technology is an emerging technology and continues to dramatically enhance healthcare by providing effective and convenient lab tools for a wide spectrum of biomedical applications, in particular for use in medical diagnostics and therapeutics. Microfluidic chip-based devices [1] provide a number of key advantages over conventional technologies, including small sample volumes (nano- to micro-liters), fast reaction times (seconds to minutes), high throughput (parallel arrangements, manifolding), salient portability, and automated handling (sample processing, mixing, reaction, and detection stages). In addition, microfluidics-based LOC devices can be mass-produced at low unit cost, making them truly disposable. These features render LOC devices an excellent candidate for the routine monitoring of public health [2-4], the environment [5], and so on.

While LOC has experienced tremendous growth and strongly impacted biomedical research over the past two decades [3], it remains limited by compatible analysis/detection platforms [6]. In parallel surface plasmon resonance (SPR) methods have shown great flexibility and robustness for detection. Specifically, nanostructured metal films that act as plasmonic sensing elements provide the fundamental technology for a new generation of SPR based assays that are emerging and compatible with microfluidic LOC platforms and highly parallel throughput studies [7].

Surface plasmons [8] (SPs) are very sensitive to the near surface dielectric constant (refractive index) and well-suited to the detection of surface binding events. The most common

methodology of SPR sensing is based on the Kretschmann configuration where a prism is used for the light-SP coupling at the surface of a thin metal film. The probe light undergoes total internal reflection on the inner surface of the prism. At a defined SPR angle, an evanescent light field travels through the thin gold film and excites SPs at the metal-dielectric interface, reducing the intensity of the reflected light. The intensities of scattered and transmitted light fields are used to determine the thickness and/or dielectric constant of the coating.

LSPR, caused by resonant SPs localized in nanostructures, have applications in near-field scanning microscopy with chemical resolution [9] and in the detection of chemical and biological agents with single molecule sensitivity [10-14]. Since researchers [15, 16] demonstrated that an array of sub wavelength holes transmits more light than predicted by classical diffraction theory [17] and correlated the extraordinary optical transmission (EOT) to the resonant excitation of surface plasmons that arise from the periodic nature of the arrays [16, 18], nanoscale metal structures have generated considerable interest. On an applied level, this work has encouraged researchers to explore the potential for creating nanoscale sensors [10-12, 14] and other devices from such arrays. Transmission mode SPR that is tailored via nanometer scale structures [19] could enable new plasmonic lab-on-chip technologies in bio/chemical sensing. The plasmonic interaction in bio/chemically functionalized nanostructure arrays may offer a new strategy for massively parallel detection of chemical and biological agents that bind to functionalized surfaces. Modulation of the nanoaperture array's optical response by adsorbed analytes is expected to offer improved sensitivity and selectivity over conventional SPR methods. In addition, by avoiding use of bulky optics and high-precision mechanics for angular or wavelength interrogation of metal films in contact with analytes, it should be possible to implement and automate the transmission SPR based sensor in compact instrumentation.

The unique optical properties of nanostructured arrays in transmission surface plasmon resonance (T-SPR) motivates further their application to surface based chemical and biological detection. In this paper, we report on the use of a nanoslit array metal film as a biosensor for detection of a retinol binding protein, β-LG. First, we investigated the correlation of the period of the nanoslit array with the primary transmission peak position and shape to select the best nanoslit array for the protein sensor. Then, self-assembled monolayers (SAMs) of alkanethiolates on the gold surfaces were used to provide a convenient way to attach a ligand receptor-retinal on the nanoslit surfaces. Additionally, integration of the nanoslit arrays with a perfusion chamber is demonstrated as a chip-based device that functions for *in-situ* surface functionalization and detection of the ligand binding protein, β-LG.

MATERIALS AND METHODS

LSPR nanoslit device design and fabrication

Nanoaperture arrays are fabricated with either a focused ion beam system (FIB) or with E-beam lithography (EBL). FIB is well suited to rapid prototyping, while EBL excels at large scale pattern generation. The finite-difference time-domain (FDTD) method was used to simulate the optical properties of metal film nanoaperture structures, giving guidance to the design and understanding to the properties of the nanoplasmonic devices that were fabricated.

In this work, we fabricated the metallic nanoslit arrays in a two-step process using standard FIB methodology. Cleaned quartz substrates were placed into an e-beam evaporator (Thermionics VE-180) and Au was evaporated thermally at a pressure of $<10^{-5}$Torr. A very thin (1-3nm) Ti layer was evaporated first to enhance the adhesion of the Au to the quartz surface. Following thin film evaporation, nanoslits were milled and a focused ion beam system (Seiko 3050SE) at 30kV accelerating voltage with a 30 – 100pA current. For a typical nanoslit array, 40 individual nanoslits were fabricated with a spacing that defined the array's periodicity. For transmission measurements, a reference window was milled into the same Au film that contains no nanoslit arrays.

Materials and functionalization of au nanoslit array

All chemicals were purchased from Aldrich-Sigma and used without further purification, if not specified otherwise. A well-established self-assembled monolayer (SAM) at gold surfaces [20,21] and chemical cross-linking reaction were used to modify the gold nanoslit surfaces for biosensor chip preparation. The retinal terminated self-assembled monolayer was prepared by the following procedure. Initially, 1 mM solution of alkanethiols (1:5mole ratio of 11-amino-1-undecanethiolto 8-hydroxy-1-octanethiol, Dojindo Molecular Technologies, Inc.) in absolute ethanol was prepared for use in preparing the first mixed alkanethiol SAM with $-NH_2$/-OH terminal moieties. Gold film nanoslit slides were incubated in the solution for 8-12 hours at room temperature. All-trans-retinal (from Sigma) was immobilized covalently to the amino-terminated SAM via formation of a Schiff's base followed by reduction with $NaCNBH_3$ (from Sigma), which is a selective reductant for imines [22]. Finally, excess trans-retinal and the reductant were removed at room temperature by extensive washing with methanol and then with acetone. The washed gold nanoslit surfaces were dried with an N_2 gas stream and then stored in the dark for the next usage.

Contact angle measurement

Contact angles were measured with sessile water drops using a home-made setup and a microscopy goniometer at room temperature in air with a humidity of 20-35%. Nearly all measurements were performed with drops that had a total volume of 10-20 microliters. The static contact angle was

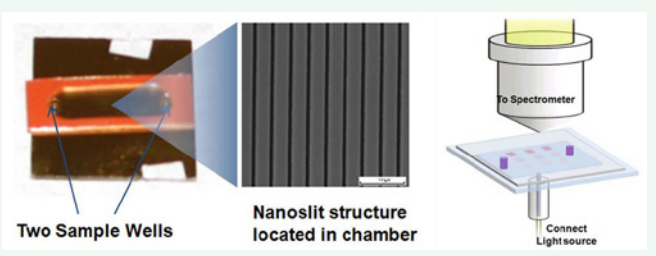

Figure 1 (Left) quartz slide with gold film coating and gold nanoslit structures in the chamber; (middle) a SEM Image of nanoslit; and (right) a schematic diagram of setup for transmission spectrum measurement.

measured after a water drop was placed on the substrate and the syringe needle was no longer touching it. Measurements were carried out for at least three drops and averaged. Each drop was made on a new spot of the substrate for each sample.

Optical measurements and setup

The EOT through the Au nanoslit array was characterized in the spectral range of 400 nm to 1800 nm, using unpolarized light at normal incidence. Transmission measurements were taken with a fiber coupled spectrometer (QE65000, Ocean Optics, or a CRAIC micro spectrophotometer). White light provided by a tungsten/halogen source was coupled into an optical fiber that was collimated and/or focused onto the nanoslit array at normal incidence. The transmitted light was collected with a high NA infinity corrected objective, collimated with the microscope optics and transmitted to a detector. Transmission data were collected as a percent transmittance or normalized to the area occupied by the nanoslits.

Figure 1 shows the experimental setup for measuring a nanoslit-based plasmonic sensor chip. A perfusion chamber is used to seal the nanoslit array, and two sample wells are used for injection of surface preparation solutions or samples for detection. The SAM preparation procedures, which were optimized on open gold surfaces, were performed in the sealed nanoslit chip in order to demonstrate the feasibility of incorporating these nanoplasmonic sensor elements into microfluidic chips. To manipulate and position the sensor, we used a control system for broad and fine adjustments within the field of view of an inverted Nikon microscope's stage. A small micro-control box for fine (micro-scale) x, y, and z translational adjustments was bolted above a large control box capable of large scale x, y, and z translational adjustments. This protocol is well-suited for a miniaturized sensor on a chip-based device.

RESULTS AND DISCUSSION

Nanoslit fabrication and optical characterization

Fabrication and Characterization: In order to study the correlation of the transmission spectra to nanoslit array periods, we fabricated gold nanoslit arrays with different periods and slit widths. The "period" is defined as the distance between nanoslits in the array; hence an increase of the period means a bigger space between two slits. Figure2 shows nanoslit structures milled within a 100 nm thick Au film with a cross section (panels (a) and (b)) for a better view of the nanoslits in the metal film. The EOT property of nanoslit array devices depends on two types of resonance waves, i.e. the SPR wave propagating along the metallic interface and the gap resonance wave inside the nanoslit cavity [15,23-25]. The wavelength of SP polaritons that are excited over the two dimensional nanoaperture array give rise to a SP resonance peak in the transmission spectrum through the nanoslit array, and the criterion for SPR is given by the phase matching condition; for the one dimensional nanoslit with normal incident light, the resonance wavelength can be approximately calculated by the equation [18]:

$$\lambda_{SPR} = P\left(\frac{\varepsilon_d \varepsilon_m}{\varepsilon_d + \varepsilon_m}\right)^{\frac{1}{2}} \quad (1)$$

where ε_d is the dielectric function of the dielectric at the metal/dielectric interface, ε_m is the metal's dielectric constant, and P is the lattice constant (period) for a square array. The resonance EOT is actually characterized by the effective refractive index(n_{eff}) at the metal/dielectric interface, the width (d) and height (h) of the slits, the period (P), and the resonance wavelength (λ) at phase matching condition [8,26]. The transmission of the gold nanoslits has a resonance wavelength given approximately by the equation [8,18,26]:

$$\lambda_{SPR} = \frac{nP}{\sqrt{1 + n_{eff}^{\ 2} / \varepsilon_m}} \quad (2)$$

The plasmon-mediated transmission is several orders of magnitude higher than expected from Bethe's law for the transmission of light through sub-wavelength apertures. The EOT spectrum is sensitive to both the geometric arrangement of the apertures in the array and the values of the dielectric functions at the metal-dielectric interface. Thus, changing the dielectric at the interface of a nanoaperture array will cause the wavelength of the transmission peak to shift, the phenomenon that we use for sensing.

A series of nanoslit arrays with different periodicity ranging from 400 nm - 1000 nm were fabricated using the FIB process. The transmission spectra are presented in Figure3a. As expected, it was found that there is a primary resonance which shifts to higher wavelength with increasing period. The change in shape of the transmission resonance is an interesting result and is indicative of the complex nature of the transmission process. The transmission spectra in Figure 3b were calculated for three different nanoslit array periodicities using the FDTD method (licensed Lumerical FDTD software). These calculations used a vacuum dielectric constant of ε_d=1 (the n_{eff} in air) and a

Figure 2 SEM images of FIB milled nanoslit arrays within a 100nm Au film: (a) 50nm slits and (b) 120nm slits as cross section view, and (c) a full view of nanoslit array. The width of the slit was controlled with the ion beam current used during fabrication.

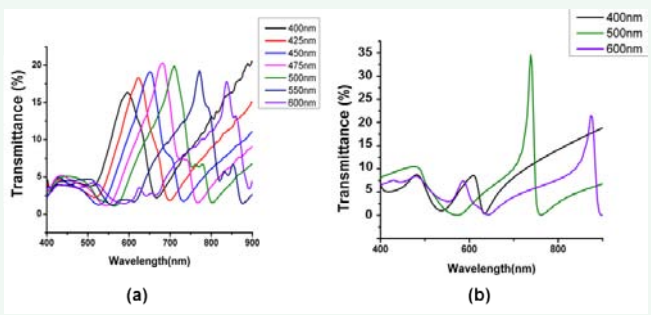

Figure 3 The measured (a) and examples of FDTD simulated (b) transmission spectra for bare Au nanoslit arrays with changing periods.

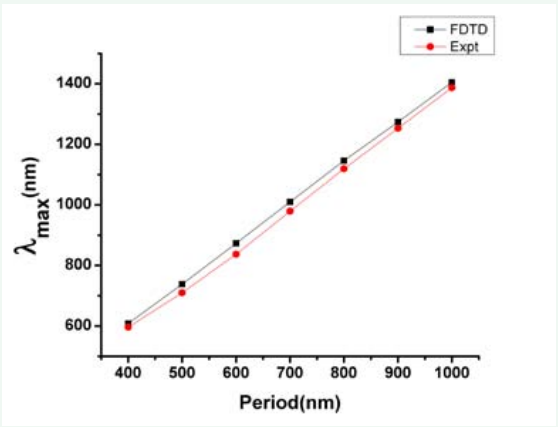

Figure 4 Correlation of λ_{max} with nanoslit array period from both the FDTD and experimental spectra.

metal dielectric constant of $\varepsilon_m \sim -12$. In general, the primary transmission peak red shifts and broadens with increasing period. The primary difference between the FDTD spectra and the transmission spectra is the overall width and definition of the peak shape. The experimental transmission peaks are broader and less well defined in general.

The wavelength of the primary transmission peak position (λ_{max}) were extracted and plotted in Figure4 for the different nanoslit periodicities, from both the FDTD and the experiment. One can find a linear correlation of the peak red-shift to the nanoslit periodicity; this work finds good agreement across all array periods. Both experimental and FDTD transmission spectra show a monotonically increasing value of λ_{max} with the period, but a broad peak width was found for bigger periods. These results indicate the importance of the nanoslit array's period in determining the transmission peak position, and thus an important parameter for bio/chemical sensor applications.

RI sensitivityof nanoslit

FDTD Simulation: A critical parameter for a nanoplasmonic sensor is the sensitivity of the resonance transmission shift to refractive index changes at or near the metal surface. In order to understand the refractive index sensing better, the profiles of the optical near field were analyzed using the FDTD method. In the simulations, the nanoslit array was chosen to have nanoslits of width 50 nm and a pitch of 2 microns (the film thickness was taken to be 100 nm). In these calculations, a single unit cell of the array was modeled and symmetric/antisymmetric boundary conditions were used to further reduce the simulation volume by a factor of four. (Note that the symmetric/anti-symmetric boundaries must be consistent with the source polarization).The simulation runs in about 5 to 15 minutes on a personal computer. Some convergence testing of the mesh size should be done for each simulation and typically mesh sizes of 5 nm or less are used for the final results.

In order to compare contributions of the shift in the peak transmission wavelength of the EOT spectrum as the refractive index changes from the metallic interface mode and the nanoslit cavity mode,the primary EOT spectra of the nanoslit with SAM modified at the top and in-gap gold surfaces are calculated respectively using the FDTD method. Figure 5 shows diagrams of the single unit cell models that were used for evaluating how the EOT spectra change with the thickness of the top organic layer (Figure 5a) and the in-gap side layer (Figure 5b); the organic layer was chosen to have a refractive index of 1.5. Figure 5c shows the electrical field intensity $|E|^2$ at the cross section of the single nanoslit unit. The calculations were used to provide spatio-temporal images of the SP dynamics (i.e., 'movies'). These visualizations provide insights into the plasmon characteristics, such as energy dissipation, decoherence, spatial propagation, and plasmon-plasmon interferences.The simulations showed a much stronger dependence of the transmitted field induced on changes in the refractive index of the side-wall inside the slit region than on the top of the nanoslit metal film.

In order to quantify the contribution of the side or top refractive index change to the EOT spectral shift, the EOT spectra were obtained at different thicknesses of the organic monolayer. Figure6a-b display the EOT spectra that were calculated for normally incident white light through the nanoslit arrays that had high refraction index regions like those shown in (Figure 5a-5b). The blue, red, and green curves in (Figure 6a) show the spectra for nanoslits coated with three different thickness layers of RI=1.5 on the top region (Figure 5a). This arrangement gives a very low RIU sensitivity. While a 2.5 nm peak shift, from 683.8 nm to 686.3 nm, is found for a 5 nm thickness coating, one only observes 0.45 nm more of a shift as the thickness increases to 30 nm. In contrast, the in-gap side-wall modification shows a large shift. Figure 6b shows the EOT peak shift of a nanoslit with the high RI layer at the side wall, and one observes 9.4, 18.9, and 45 nm peak shifts for the layer thicknesses 5, 10, 30 nm, respectively. These results suggest that dominant contribution to the surface plasmon induced EOT peak shift is caused by the refractive index changes from the side-wall of the nanoslit (cavity mode), which is in agreement with previous theoretical studies [27].

Experimental RI Sensitivity: The effect of increasing the refractive index of the dielectric on the EOT peak wavelength shift was tested in experiments. The refractive index changes were obtained using water-methanol solvent mixtures; the refractive indices were pure water (RI=1.3355), 20% methanol (RI=1.3380), and 40% methanol (RI=1.3415). The nanoslit array was immersed in the above solvents and the EOT spectra were recorded to obtain the primary EOT resonance peak shift. The peakshift to the refractive index changes gives an RI sensitivity of 626nm/RIU. This sensitivity is in reasonable agreement with that obtained for SAM coated nanoslit surfaces [27] and higher than most nanoparticle-based LSPR sensitivity [28-30].

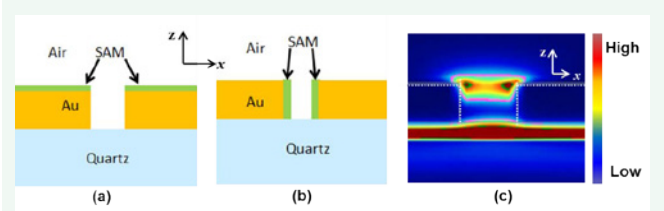

Figure 5 Panel a-b: The configuration of the metal film with surface modifications used for FDTD simulation; Panel c: a snapshot of the electrical field intensity $|E|^2$ at the cross section of the single nanoslit unit from FDTD simulation.

Surface functionalization and characterization

In order to detect the binding of targeted analytes, the Au surface of the nanoslit must be functionalized with receptors that are highly selective for the analyte. In this work, a retinal-binding protein, β-LG, was used as the targeting protein, and a self-assembled monolayer (SAM) of tethered retinal groups was prepared at the nanoslit array surface. The step-wise preparation of the retinal terminated SAM is schematically illustrated in (Figure 7). First, a SAM with an $-NH_2$ terminal moiety was formed at the gold surface. Then, the all-trans-retinal was immobilized covalently to the amino-terminated SAM via formation of a Schiff base, and it was followed by reduction with $NaCNBH_3$, which is a selective reductant for imines. In the last step, excess trans-retinal and reductant were removed at room temperature by extensive washing with methanol and then with acetone. The washed gold nanoslit surfaces were air dried and used for characterization and testing.

Contact angle measurements: To assess consistency in the SAM preparation and retinal attachment, water drop contact angles were measured after each preparation step using gonionometry, as well as after the ligand protein binding reactions. A contact angle of a droplet on a surface reflects the balance of interfacial free energy between the three interacting phases: the substrate, the liquid, and air. A surface with a contact angle less than 90° is considered to be hydrophilic and a surface with a contact angle greater than 90° is considered to be hydrophobic. At the extremes of 0° and 180°, the surface is considered completely wetted or not wetted at all, respectively. With the contact angle measurement, we can simply and directly evaluate the SAM preparation on the surface.

Table 1 presents the resulting static contact angles for a gold surface, a gold surface after the SAM of $-NH_2$/-OH, after covalently grafting retinal to $-NH_2$, and after two ligand proteins (β-LG or α-LG) binding interactions. Because of the$-NH_2$/-OH moieties of the SAM are more hydrophilic than pure gold surfaces, the contact angle to water decreases from the bare gold surface. The contact angle increases when the hydrophobic retinal is bound to the $-NH_2$ moieties at the surface. This behavior demonstrates the surface modification and is consistent with expectation.

Because the β-LG has a unique specific binding affinity to the small hydrophobic retinal groups [31] while α-LG does not, the α-LG provides a useful control assay for nonspecific binding. The significant contact angle difference of the β-LG binding as compared to the α-LG binding (34 vs. 2 degrees, respectively) indicates the specific affinity of β-LG to retinal tethered SAM.

Chip-based nanoslit array for protein detection

As the most abundant whey protein in bovine milk, β-LG

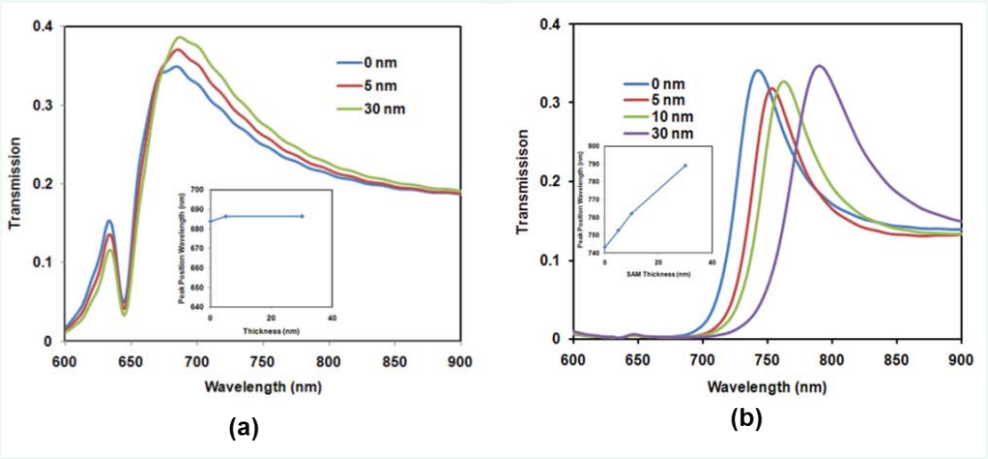

Figure 6 Results of optical transmission through an Au nanoslit array through the FDTD calculation: (a) the top organic SAM layer only and (b) in-gap side wall only. The SAM thickness is changed from 0 to 30 nm. The insert figure shows the peak shift vs. the thickness of adsorbed organic layer.

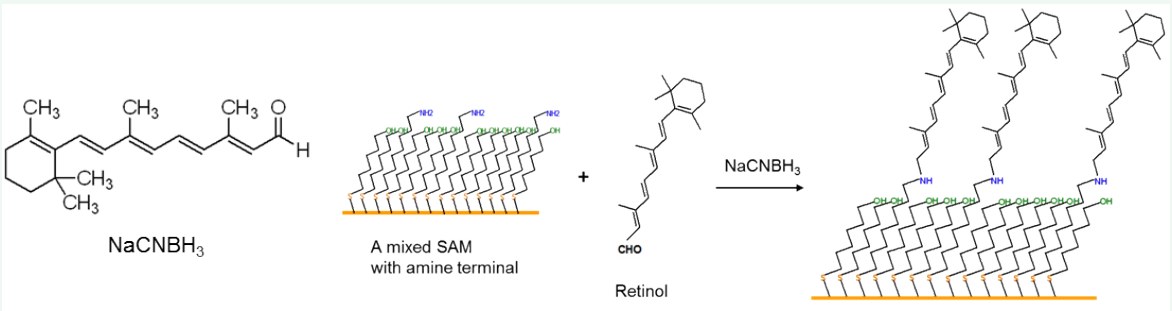

Figure 7 A schematic procedure for the retinal SAM preparation: The left is the structure of retinal; the right panel shows the reaction of attaching retinal to the amino-terminated SAM.

Table 1: Static water contact angles of different surfaces.

Surface	Au film	NH_2/OH SAM	Retinal SAM	β-LG (0.5 mg/mL)	α-LG (0.5 mg/mL)
Contact angle	64±3	50±1	80±2	46±2	77±3

plays an important role in the processing of dairy foods, due to its unique structural characteristics [32] which include a buried sulfhydryl group that becomes exposed during thermal denaturation [33]. As seen in the contact angle study, β-LG binds to the immobilized retinal moieties with high specificity. Therefore, taking advantage of this property, we developed a bio-selective transmission SPR model sensor for β-LG detection using the developed metal film nanoslit array.

The nanoslit array (400 nm periods, 50 nm slit) of the primary transmission peak around 680 nm was used to detect the β-LG protein. First we studied the saturation binding of β-LG to retinal sites at the nanoslit array by incubating the nanoslit array chip in a 200μg/mL of β-LG in a 20 mM pH 5.4 PBS. We selected a pH=5.4 value because of the optimal retention time during binding interactions [34]. The nanoslit slide was rinsed with the pH=5.4 PBS buffer and dried under an N_2 stream before measuring the EOT spectrum measurement in air. Figure 8 shows a well-defined EOT spectrum for normally incident white light through the nanoslit array after successive surface modifications. The transmission peak intensities have been scaled to the same maximum value for easier comparison. The blue and red curves exhibit the spectra for the all-trans-retinal coated nanoslits after the incubation with the retinal binding protein, in the 200μg/mL β-LG solution (from bovine milk ~ 90%) for 10 min. We found a 10.8 nm peak shift from 672.5nm to 683.3nm after the β-LG binding on the nanoslit; presumably this time is enough to reach binding equilibrium (because of no extra peak shift with longer incubation time).

The peak shift in the transmission SPR shown in (Figure 8) is related to changes in the effective dielectric constant (refractive index) at the metallic nanoslit array interface. By assuming that the total change comes from increasing the organic layer thickness, the effective dielectric constant at the modified interface can be calculated according to reference [35]. From the above measured bulk RI sensitivity of 626 nm/RIU, one is able to estimate the effective thickness of β-LG attached to the retinal

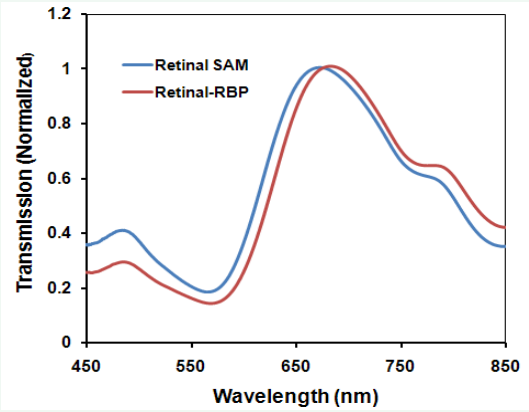

Figure 8 Optical transmission through an Au nanoslit array: Retinal SAM (blue) and after β-LG binding (red).

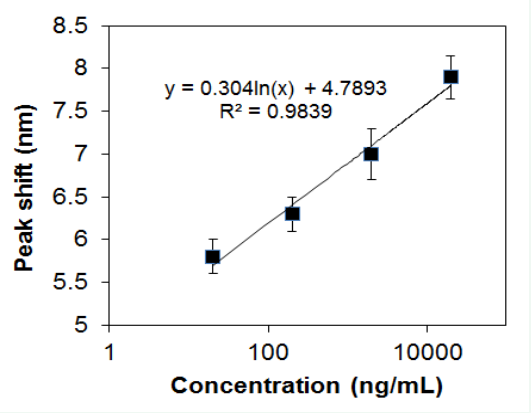

Figure 9 Detection of β-LG in PBS electrolyte solution: the dependence of the wavelength peak shift on the β-LG concentration.

SAM surfaces according to the equation [35-37]:

$$\Delta R = m(n_{\beta-LG} - n_{Air})[\exp(-2d_{SAM}/l_d)][1-\exp(-2d_{\beta-LG}/l_d)] \quad (3)$$

in which the ΔR (10.8 nm) is the peak shift after the protein binding on the retinal SAM, d_{SAM} is the effective thickness of the retinal monolayer (~ 2.1 nm), l_d is the decay length of SP mode into the dielectric at the nanoslit array, l^d = 30 nm [27] is used), and refractive indices of organic molecules is taken to be 1.5 and that of air is 1.0. With these values, the increase in the layer thickness at the nanoslit surfaces is found to be 0.7 nm. Assuming that all of this increase comes from β-LG adsorption, taking its molecular weight to be 18.4 kDa, and using a globular diameter of 1.6-1.9 nm [38], the coverage of the protein at the nanoslit surface is 37% to 44% of full coverage. This result is reasonable because the retinal sites are limited or the sites at nanoslit array might not be fully used because of steric effects or double-layer hindrance [39, 40] of the narrow nano-gap.

The β-LG protein detection at the sealed perfusion chamber (Figure 1) was performed to demonstrate the capability of direct chip-based bio-detection of β-LG protein. Various concentrations of β-LG in pH 5.4 PBS were syringed in the chamber into which a nanoslit sensor was sealed and the flow was stopped for 10 minutes. Thereafter the analyte solution was syringed out, rinsed with DI water, and dried with N_2 streaming before collecting the transmission spectra at individual concentrations.

Figure 9 shows the dependence of the wavelength peak shift on the β-LG concentration. The peak shift for each point was obtained by averaging three measurements. As expected, the primary resonance peak red shifts when the nanoslit array is exposed to β-LG, and the red shift increases with increasing β-LG concentration [27,35].The linear fit of the peak shift with logarithmic value of the β-LG concentration gives an R^2 value of 0.984 (corresponding to concentration ranges of20 ng/mL to 20μg/mL). These results indicate that the nanoslit platform, along with tailored surface modification with appropriate receptors,

can be used as protein sensors with high sensitivity. More research on different protein detection (in particular for health care monitoring, e.g. biomarkers of diseases) in an integrated chip device with a microfluidics system, including sample preparation and automated operation are under investigation.

CONCLUSION

In summary, a metal film nanoslit array has been investigated as a transmission mode SPR biosensor by utilizing its extraordinary optical transmission spectrum. Finite-difference time-domain (FDTD) simulation studies have shown that the nanoslit array device provides a well-defined transmission resonance that is tunable from the visible to the near infrared. A consistent red shift of the primary SPR transmission peak was observed as the refractive index increases, validating the use of this nanoplasmonics-based platform for quantitative detection of analyte binding that causes refractive index changes. The FDTD simulation revealed that the red shift of EOT peak results mostly from the dielectric constant changes in the nanoslit region, the side wall surfaces, rather than the top surfaces.The bulk refractive index sensitivity of a 400 nm period nanoslit array is found to be 626nm/RIU, which is higher than most gold nanoparticle-based LSPR sensors on planar substrates. The nanoslit array demonstrates an integration of on-chip sensitive detection of β-LG with a modified retinal monolayer in a transmission SPR mode, suggesting compatibility to microfluidics and emerging miniaturized lab-on-chip biosensor application.

ACKNOWLEDGEMENTS

This project was financially supported by NASA grant (contract: NNX08CD36P) and by NIH grant (contract: 1R43CA153899-01). Wei thanks the support from JSNN.

REFERENCES

1. Haeberle S, Zengerle R. Microfluidic platforms for lab-on-a-chip applications. Lab Chip. 2007; 7: 1094-1110.
2. Foudeh AM, Fatanat Didar T, Veres T, Tabrizian M. Microfluidic designs and techniques using lab-on-a-chip devices for pathogen detection for point-of-care diagnostics. Lab Chip. 2012; 12: 3249-3266.
3. Lei KF. Microfluidic systems for diagnostic applications: a review. J Lab Autom. 2012; 17: 330-347.
4. Lin CC, Tseng CC, Chuang TK, Lee DS, Lee GB. Urine analysis in microfluidic devices. Analyst. 2011; 136: 2669-2688.
5. Ward N, Mu X, Serrano G, Covington E, Kurdak C, Zellers ET, et al. Microfluidic-packaged CMOS chemiresistor detector for micro-scale gas chromatograph. Micro & Nano Letters. 2012; 7: 721-724.
6. Hill D, Sandstrom N, Gylfason K, Carlborg F, Karlsson M, Haraldsson T, Sohlstrom H. Microfluidic and transducer technologies for lab on a chip applications. Conf Proc IEEE Eng Med Biol Soc. 2010; 2010: 305-307.
7. Hoa XD, Kirk AG, Tabrizian M. Towards integrated and sensitive surface plasmon resonance biosensors: a review of recent progress. Biosens Bioelectron. 2007; 23: 151-160.
8. Raether H. Surface Plasmons on Smooth and Rough Surfaces and on Gratings. Springer Berlin Heidelberg. 1988.
9. Song Y, Nallathamby PD, Huang T, Elsayed-Ali HE, Xu X-HN. Correlation and Characterization of Three-Dimensional Morphologically Dependent Localized Surface Plasmon Resonance Spectra of Single Silver Nanoparticles Using Dark-Field Optical Microscopy and Spectroscopy and Atomic Force Microscopy. J. Phys. Chem. C. 2010; 114: 74-81.
10. Stewart ME, Anderton CR, Thompson LB, Maria J, Gray SK, Rogers JA, et al. Nanostructured plasmonic sensors. Chem Rev. 2008; 108: 494-521.
11. Spoto G, Minunni M. Surface Plasmon Resonance Imaging: What Next? J. Phys. Chem. Lett. 2012; 3: 2682-2691.
12. Valsecchi C, Brolo AG. Periodic metallic nanostructures as plasmonic chemical sensors. Langmuir. 2013; 29: 5638-5649.
13. Frolov L, Dix A, Tor Y, Tesler AB, Chaikin Y, Vaskevich A, et al. Direct observation of aminoglycoside-RNA binding by localized surface plasmon resonance spectroscopy. Anal Chem. 2013; 85: 2200-2207.
14. Mayer KM, Hafner JH. Localized surface plasmon resonance sensors. Chem Rev. 2011; 111: 3828-3857.
15. Ebbesen TW, Lezec HJ, Ghaemi HF, Thio T, Wolff PA. Extraordinary optical transmission through sub-wavelength hole arrays. Nature. 1998; 391: 667-669.
16. Ghaemi HF, Thio T, Grupp DE, Ebbesen TW, Lezec HJ. Surface plasmons enhance optical transmission through subwavelength holes. Phy.Rev. B. 1998; 58: 6779-6782.
17. Bethe HA. Theory of Diffraction by Small Holes. Phy.Rev. 1944; 66: 163.
18. Thio T, Ghaemi HF, Lezec HJ, Wolff PA, Ebbesen TW. Surface-plasmon-enhanced transmission through hole arrays in Cr films. J Opt Soc Am B. 1999; 16: 1743-1748.
19. Barnes WL, Dereux A, Ebbesen TW. Surface plasmon subwavelength optics. Nature. 2003; 424: 824-830.
20. Wei J, Liu H, Dick AR, Yamamoto H, He Y, Waldeck DH. Direct wiring of cytochrome c's heme unit to an electrode: electrochemical studies. J Am Chem Soc. 2002; 124: 9591-9599.
21. Liu H, Yamamoto H, Wei J, Waldeck DH. Control of the Electron Transfer Rate between Cytochrome c and Gold Electrodes by the Manipulation of the Electrode's Hydrogen Bonding Character. Langmuir. 2003; 19: 2378-2387.
22. Lane CF. Sodium Cyanoborohydride - A Highly Selective Reducing Agent for Organic Functional Groups. Synthesis. 1975; 1975: 135-146.
23. Skorobogatiy M, Kabashin AV. Photon crystal waveguide-based surface plasmon resonance biosensor. Appl. Phys. Lett. 2006; 89: 143518.
24. Caglayan H, Ozbay E. Surface wave splitter based on metallic gratings with sub-wavelength aperture. Opt Express. 2008; 16: 19091-19096.
25. Lalanne P, Hugonin JP, Rodier JC. Theory of surface plasmon generation at nanoslit apertures. Phys Rev Lett. 2005; 95: 263902.
26. Lalanne P, Sauvan C, Hugonin JP, Rodier JC, Chavel P. Perturbative approach for surface plasmon effects on flat interfaces periodically corrugated by subwavelength apertures. Phys. Rev. B. 2003; 68: 125404.
27. Jung YS, Sun Z, Wuenschell J, Kim HK, Kaur P, Wang L, et al. High-sensitivity surface plasmon resonance spectroscopy based on a metal nanoslit array. Appl. Phys. Lett. 2006; 88: 243105.
28. Gish DA, Nsiah F, McDermott MT, Brett MJ. Localized surface plasmon resonance biosensor using silver nanostructures fabricated by glancing angle deposition. Anal Chem. 2007; 79: 4228-4232.
29. Jung S, Shuford KL, Park S. Optical Property of a Colloidal Solution of Platinum and Palladium Nanorods: Localized Surface Plasmon

Resonance. J. Phys. Chem. C. 2011; 115: 19049-19053

30. Juvé V, Cardinal MF, Lombardi A, Crut A, Maioli P, Pérez-Juste J, et al. Size-dependent surface plasmon resonance broadening in nonspherical nanoparticles: single gold nanorods. Nano Lett. 2013; 13: 2234-2240.

31. Kontopidis G, Holt C, Sawyer L. Invited review: beta-lactoglobulin: binding properties, structure, and function. J Dairy Sci. 2004; 87: 785-796.

32. Kontopidis G, Holt C, Sawyer L. The ligand-binding site of bovine beta-lactoglobulin: evidence for a function? J Mol Biol. 2002; 318: 1043-1055.

33. Sawyer L, Brownlow S, Polikarpov I, Wu S-Y. ß-Lactoglobulin: Structural Studies, Biological Clues. International Dairy Journal. 1998; 8: 65-72.

34. Wang Q, Swaisgood HE. Characteristics of beta-lactoglobulin binding to the all-trans-retinal moiety covalently immobilized on Celite. J Dairy Sci. 1993; 76: 1895-1901.

35. Jung LS, Campbell CT, Chinowsky TM, Mar MN, Yee SS. Quantitative Interpretation of the Response of Surface Plasmon Resonance Sensors to Adsorbed Films. Langmuir. 1998; 14: 5636-5648.

36. Haemers S, Koper GJM, van der Leeden MC, Frens G. An Alternative Method To Quantify Surface Plasmon Resonance Measurements of Adsorption on Flat Surfaces. Langmuir. 2002; 18: 2069-2074.

37. Haes AJ, Van Duyne RP. A unified view of propagating and localized surface plasmon resonance biosensors. Anal Bioanal Chem. 2004; 379: 920-930.

38. Erickson HP. Size and Shape of Protein Molecules at the Nanometer Level Determined by Sedimentation, Gel Filtration, and Electron Microscopy. Biol Proced Online. 2009; 11: 32-51.

39. Pennathur S, Santiago JG. Electrokinetic transport in nanochannels. 1. Theory. Anal Chem. 2005; 77: 6772-6781.

40. Karnik R, Fan R, Yue M, Li D, Yang P, Majumdar A. Electrostatic Control of Ions and Molecules in Nanofluidic Transistors. Nano Letters. 2005; 5: 943-948.

Cite this article

Wei J, Kofke M, Singhal S, Waldeck DH (2014) A Study of Localized Surface Plasmon Resonance Nanoslit Array and Applications for Chip-based Protein Detection. JSM Nanotechnol Nanomed 2(2): 1024.